

Article

Laboratory Study of Effective Stress Coefficient for Saturated Claystone

Fanfan Li ^{1,2,*}, Weizhong Chen ³, Zhigang Wu ², Hongdan Yu ³, Ming Li ², Zhifeng Zhang ² and Fusheng Zha ¹¹ School of Resources and Environmental Engineering, Hefei University of Technology, Hefei 230009, China² Research and Development Center on Technology and Equipment for Energy Conservation and Environmental Protection of Highway Transport, Anhui Transport Consulting & Design Institute Co., Ltd., Hefei 230088, China³ State Key Laboratory of Geomechanics and Geotechnical Engineering, Institute of Rock and Soil Mechanics, Chinese Academy of Sciences, Wuhan 430071, China

* Correspondence: lifanfan@acdi.ah.cn

Abstract: Claystone is potentially the main rock formation for the deep geological disposal of high-level radioactive nuclear waste. A major factor that affects the deformation of the host medium is effective stress. Therefore, studying the effective stress principle of claystone is essential for a stability analysis of waste disposal facilities. Consolidated drained (CD) tests were carried out on claystone samples to study their effective stress principle in this paper. Firstly, two samples were saturated under a specified confining pressure and pore pressure for about one month. Secondly, the confining pressure and pore pressure were increased to a specified value simultaneously and then reverted to the previous stress state (the deformations of the samples were recorded during the whole process). Different incremental combinations of the confining pressure and pore pressure were tried at this step. Finally, the effective stress coefficients of the samples were obtained through a back analysis. Furthermore, some potential influencing factors (the neutral stress and loading rate) of the effective stress coefficient were also studied through additional tests. Some interesting results are worth mentioning: (1) the effective stress coefficient of claystone is close to one; (2) the neutral stress and loading rate may have little effect on the effective stress coefficient of claystone.

Keywords: claystone; effective stress; consolidated drained; back analysis; loading–unloading cycles; neutral stress; loading rate



Citation: Li, F.; Chen, W.; Wu, Z.; Yu, H.; Li, M.; Zhang, Z.; Zha, F. Laboratory Study of Effective Stress Coefficient for Saturated Claystone. *Appl. Sci.* **2023**, *13*, 10592. <https://doi.org/10.3390/app131910592>

Academic Editor: Nikolaos Koukouras

Received: 5 August 2023

Revised: 11 September 2023

Accepted: 19 September 2023

Published: 22 September 2023



Copyright: © 2023 by the authors. Licensee MDPI, Basel, Switzerland. This article is an open access article distributed under the terms and conditions of the Creative Commons Attribution (CC BY) license (<https://creativecommons.org/licenses/by/4.0/>).

1. Introduction

As a potential host medium for the deep geological disposal of radioactive nuclear waste, claystone is found under highly complex hydro-mechanical (HM) conditions [1]. Therefore, studying the stress–strain laws of claystone under HM conditions is essential for the stability analysis of radioactive waste disposal repositories. Because of its important role in the stress–strain laws of a geomaterial, the effective stress principle of claystone was studied in this paper.

Effective stress was first proposed by Terzaghi [2], who considered that pore pressure could counteract total stress. The effective stress principle satisfies the following form:

$$\sigma_e = \sigma - \sigma_p \quad (1)$$

where σ_e is the effective stress, σ is the total stress, and σ_p is the pore pressure.

However, Biot [3] found that Terzaghi's effective stress principle was unsuitable for porous media with low permeability and believed that pore pressure could not offset the total pressure in a 1:1 ratio. A modified effective stress principle was proposed as follows [3]:

$$\sigma_e = \sigma - \eta\sigma_p \quad (2)$$

where η is the effective stress coefficient of a geomaterial.

Since Biot [3] modified the effective stress principle, numerous studies have investigated it in different soils and rocks [4–8]. Table 1 presents a summary of the various equations used in the literature for the effective stress principle.

Table 1. Effective stress principle of references.

| References | Effective Stress | Related Research Work |
|-----------------------------|--|---|
| Nur and Byerlee [9] | Saturated: $\eta = 1 - (K/K_s)$; K is the bulk moduli of rock; K_s is the bulk moduli of grain. | The rock strain was quantified based on this effective stress principle, and its validity was verified via compression test results of sandstone and granite. |
| Zoback and Byerlee [10] | Saturated: A variable greater than 1 and varies with stress. | The phenomenon that pore pressure has a greater impact on permeability than confining pressure was found according to the permeability test results of sandstone under different confining and pore pressures. |
| Berryman [11] | Saturated: $\eta = \frac{K}{K^{(1)} - K^{(2)}} (\eta^{(1)} - \eta^{(2)}) + \theta$; K is the bulk modulus of drained porous frame; $K^{(1)}$ and $K^{(2)}$ are the drained frame moduli of porous constituents (1) and (2); $\eta^{(1)}$ and $\eta^{(2)}$ are the effective stress coefficient of porous constituents (1) and (2); θ is the relative change in the effective stress coefficient for a two-component porous medium. | The effective stress coefficients of a two-component porous medium are deduced based on the existing research work, and the phenomenon of Zoback and Byerlee [10] is explained based on this conclusion. |
| Tuncay and Corapcioglu [12] | Saturated: $\sigma_e = \sigma - \eta_1 \sigma_p^f - \eta_2 \sigma_p^p$; $\eta_1 = \frac{(1-\alpha_f)K_{fr}}{K_{fr}^m} - 1$; $\eta_2 = \frac{K_{fr}}{K_s} - \frac{(1-\alpha_f)K_{fr}}{K_{fr}^m}$; η_1 is the effective stress coefficient for the fractures; η_2 is the effective stress coefficient for the pores; σ_p^f is the pore pressure in the fractures; σ_p^p is the pore pressure in the pores; α_f is the volume fraction of the fractures; K_s is the bulk moduli of grain; K_{fr} is the drained bulk modulus of the fractured porous medium; K_{fr}^m is the drained bulk modulus of the nonfractured porous medium. | An effective stress principle for saturated fractured porous media is proposed based on the assumption of linear elasticity. |
| George and Barakat [13] | Saturated: $\eta = 0.71$; | A series of loading–unloading (both total stress and pore pressure) cycles applied by gas pressure were performed on the coal specimen, and the effective stress coefficient was obtained. |
| Kwon et al. [14] | Saturated: $\eta = -\frac{\partial \log k / \partial \sigma_p}{\partial \log k / \partial \sigma}$; k is the permeability. | The effective stress coefficient of illite-rich shale was determined according to the transient pulse test results of saturated samples. |
| Tsuji et al. [15] | Saturated: Terzaghi’s effective stress principle. | A theoretical relationship between the acoustic velocity and mean effective stress of the Nankai accretionary prism was calculated using DEM (Differential Effective Medium) theory and the aspect ratio spectrum of pore space, and Terzaghi’s effective stress principle was introduced to analyze the pore pressure distribution of Nankai trough. |
| Bagherieh et al. [16] | Unsaturated: $\sigma_e = \sigma - \alpha_m [\chi_m u_{mw} + (1 - \chi_m) u_{ma}] I - \alpha_M [\chi_M u_{Mw} + (1 - \chi_M) u_{Ma}] I$ $\chi_m = \begin{cases} \left(\frac{S_{m(e)}}{u_{ma} - u_{mw}} \right)^\Omega & \text{for } S_m \geq S_{m(e)} \\ 1 & \text{for } S_m \leq S_{m(e)} \end{cases} ;$ $\chi_M = \begin{cases} \left(\frac{S_{M(e)}}{u_{Ma} - u_{Mw}} \right)^\Omega & \text{for } S_M \geq S_{M(e)} \\ 1 & \text{for } S_M \leq S_{M(e)} \end{cases}$ u_{mw} , u_{ma} , u_{Mw} , and u_{Ma} are the micropore water, micropore air, macro pore water, and macro pore air pressures; α_m and α_M are the conventional effective stress coefficients of saturated double-porous media; $S_{m(e)}$ is the suction value separating saturated from unsaturated conditions in the micropores; $S_{M(e)}$ is the matric suction value separating saturated from unsaturated conditions in the macro pores; Ω is the material parameter. | Drying and one-dimensional consolidation tests are performed on initially saturated samples of the kaolin (double-porosity compacted soil) at different net stresses, and the test results were accurately predicted using the new effective stress principle. |
| Chabezloo et al. [2] | Saturated: $\eta = c\sigma_d + d$; c and d are the fitting parameters; σ_d is the differential stress. | The effective stress law for the permeability of limestone is studied by drained hydrostatic compression and constant-head permeability tests, and the results show that the effective stress coefficient was linearly related to differential stress. |

Table 1. Cont.

| | | |
|-----------------------------------|--|---|
| <p>Nowamooz et al. [17]</p> | <p>Unsaturated: $\sigma = \sigma_c + \sigma_a + \eta(\sigma_w - \sigma_a)$; $\eta = \frac{\tan \phi^b}{\tan \phi^l}$; σ_w is the pore water pressure; σ_a is the pore air pressure; ϕ^b is the angle indicating the increase in the matrix suction's shear stress function; ϕ^l is the lowest matrix suction.</p> | <p>The effective stress law of compacted natural clay sand in Missillac was obtained using the direct shear test and the soil water retention curve (SWRC), and its validity was verified by simulating the resilient behavior of repeated-load triaxial tests.</p> |
| <p>Konrad and Lebeau [18]</p> | <p>Unsaturated: $\sigma = \sigma_c + \sigma_a + \eta(\sigma_w - \sigma_a)$; $\eta = A_{Sr} + \frac{e^* B}{2 \cos \theta}$; A_{Sr} is the fraction of the fracture surface wetted by water; e^* is the maximum local aperture currently occupied by water; B is the total perimeter of water menisci between two fracture walls; θ is the contact angle of the fracture water.</p> | <p>The effective stress equation is derived for partially saturated rough-walled fractures with any aperture distributions based on the capillary law, and the nonlinearity of the effective stress parameter versus the saturation degree curves is found to be mainly determined by the surface roughness (or the coefficient of variation) rather than the mean aperture of the fractures.</p> |
| <p>Zhang [19]</p> | <p>Saturated: $\sigma A = \sigma_{is} A_s + \sigma_l A_l + \sigma_p A_p$; σA is the total normal force externally applied on the surface A; $\sigma_{is} A_s$ is the total normal force acting on the solid–solid contact area, A_s, with the local total stress σ_{is}; $\sigma_l A_l$ is the total normal repulsive force acting in the water–film section, A_l, between clay particles, with the local total pressure σ_l; $\sigma_p A_p$ is the pressure σ_p acting on the surface A_p in the large pores occupied by free water.</p> | <p>The effective stress in a dense clay–water system is transferred through both the adsorbed interparticle porewater in narrow pores and the solid–solid contact between non-clay mineral grains. This concept has been widely validated by various kinds of experiments performed on the COX and OPA claystones.</p> |
| <p>Saurabh and Harpalani [20]</p> | <p>Unsaturated: $\sigma_{11} = C_{11} \epsilon_{11} + C_{12} \epsilon_{22} + C_{12} \epsilon_{33} - \eta_1 p_c - (1 - \eta_1) s_m^{\alpha_1}(p)$ $\sigma_{22} = C_{12} \epsilon_{11} + C_{11} \epsilon_{22} + C_{13} \epsilon_{33} - \eta_1 p_c - (1 - \eta_1) s_m^{\alpha_1}(p)$ $\sigma_{33} = C_{13} \epsilon_{11} + C_{13} \epsilon_{22} + C_{33} \epsilon_{33} - \eta_3 p_c - (1 - \eta_3) s_m^{\alpha_3}(p)$ $\sigma_{23} = 2C_{44} \epsilon_{23}; \sigma_{31} = 2C_{44} \epsilon_{31}; \sigma_{12} = 2 \frac{C_{11} - C_{12}}{2} \epsilon_{12}$; $\eta_1 = \frac{C_{13} \frac{d\epsilon_3}{dp} - \frac{d\sigma_{11}}{dp} - \frac{ds_m^{\alpha_1}(p)}{dp}}{1 - \frac{ds_m^{\alpha_1}(p)}{dp}}; \eta_3 = \frac{C_{33} \frac{d\epsilon_3}{dp} - \frac{ds_m^{\alpha_3}(p)}{dp}}{1 - \frac{ds_m^{\alpha_3}(p)}{dp}}$; σ_{ij}, ϵ_{ij} and C_{ij} are the total stress, compliance matrix, and strain along the $i - j$ direction, respectively; η_1 and η_3 are the effective stress coefficients of transversely isotropic media; p is the pore pressure; p_c is the pore pressure in the cleat system of media; $s_m^{\alpha}(p)$ is a pressure-dependent quantity coupling the sorption-based stress and strain in a microporous media.</p> | <p>The estimated values of the effective stress coefficients in both the vertical and horizontal directions are different, varying with pressure for methane depletion, and a conceptual physical model of effective stress, which considered absorption, was proposed.</p> |
| <p>Ma et al. [21]</p> | <p>Saturated: $\sigma_c = a\sigma_p^2 - (a\sigma + b)\sigma_p + \sigma$; a and b are the fitting parameters.</p> | <p>A series of flow-through experiments consisting of three continuous stages (pre-reaction stage, reaction stage, and post-reaction stage) were conducted, and the cross-plot method was introduced to determine the effective law of tight sandstone with mineral dissolvable mineral.</p> |
| <p>Civan [22]</p> | <p>Saturated: $\frac{\eta}{1-\eta} = a \left(\frac{K}{\phi} \right)^b$; a and b are the fitting parameters; K is the intrinsic permeability of porous rock; ϕ is the porosity of porous formation.</p> | <p>The modified power-law equation yields a physically meaningful correlation because it successfully satisfies the low-end- and high-end-limit values of the effective stress coefficient and also provides a better quality match of the available experimental data than the semilogarithmic equation and the popular basic power-law equation.</p> |
| <p>Zhao et al. [23]</p> | <p>Saturated: $\eta = \begin{cases} \frac{1}{1 + \frac{\sigma - \sigma_p}{k_{n0} u_{nmax}}} & \sigma \geq \sigma_p \\ 1 & \sigma < \sigma_p \end{cases}$; k_{n0} is the initial normal stiffness; u_{nmax} is the maximum fracture closure.</p> | <p>A new effective stress coefficient model for single rough water-bearing fractures is proposed in terms of initial normal stiffness and maximum normal closure, and it was verified by laboratory and in situ experimental data.</p> |

The theoretical derivation and empirical formula are the two main expressions of the effective stress principle. The advantage of the theoretical derivation is that an equation that is more consistent with the physical principles can be obtained, but the disadvantage is that some physical quantities in the equation are difficult to measure. The accuracy of the empirical formula is related to the measured physical parameter (the permeability coefficient is favored), which is related to the effective stress coefficient. The adverse effects caused by water pressure changes (the permeability test requires a head difference between the upstream and downstream of the sample) in the permeability test are difficult to evaluate. In this study, the CD tests were conducted to measure the effective stress coefficient of claystone. The samples were firstly saturated under an in situ stress state for about one month. Then the effective stress coefficients were checked by changing the confining pressure and pore pressure in specific increments (the deformations of the samples were recorded during the whole process). Different increments of pore pressure and confining pressure were tried during the effective stress coefficient checking procedures, and an accurate conclusion was obtained through a back analysis (the effective stress

coefficient was 0.991 for sample one and 0.995 for sample two). At last, some factors potentially influencing the effective stress principle of claystone were tested and discussed.

2. Experimental Testing

2.1. Experimental Device

The CD tests were performed on a parallel-linkage triaxial testing machine designed by the Institute of Rock and Soil Mechanics, Chinese Academy of Sciences. This machine can implement the mechanical tests simultaneously for two samples with the same confining pressures, the same pore pressures, and different axial pressures. The double-linkage triaxial testing machine is shown in Figure 1a, and the schematic diagram of the increase/decrease in the specimen's confining, axial, and pore pressure is shown in Figure 1b. The deformations of the samples were measured by the LVDT (Linear Variable Differential Transformer), and the accuracy of the LVDT achieved was 10^{-7} m.

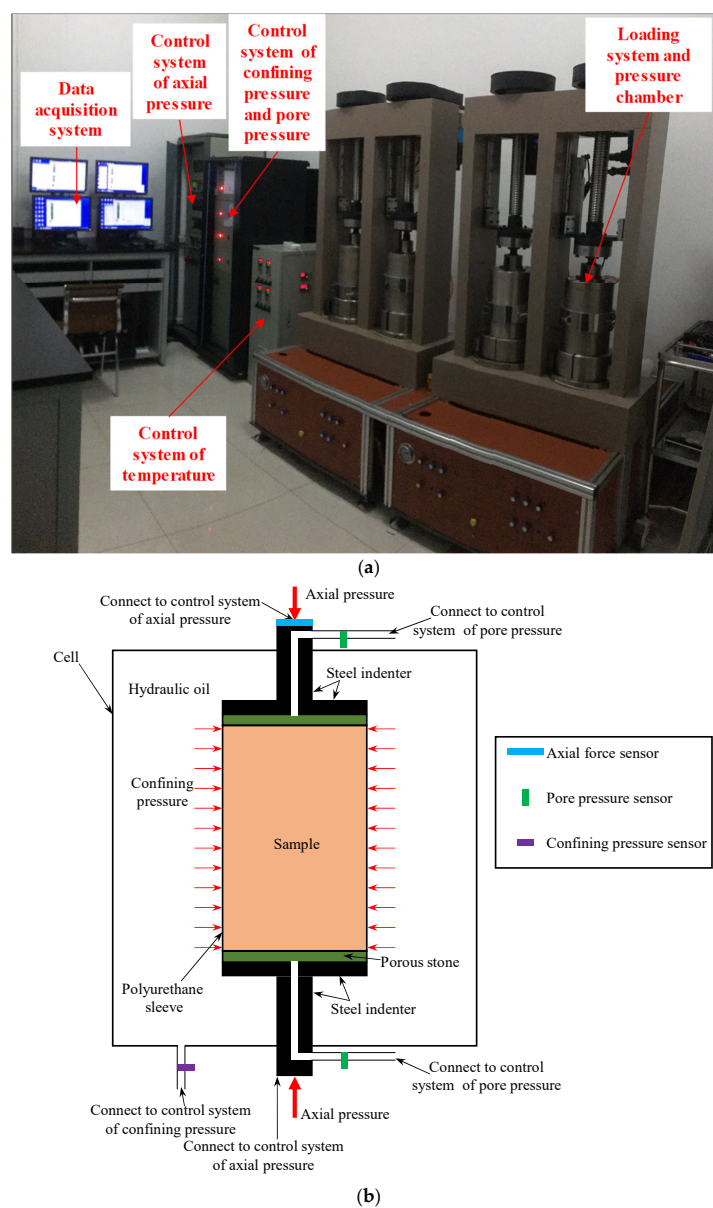


Figure 1. Double-linkage triaxial testing machine: (a) actual test equipment; (b) test equipment schematic diagram.

2.2. Samples' Preparation and Basic Properties

The adequate claystone samples in this study were trimmed from blocks extracted at a depth of 223 m [24] (the effective stress is about 2.5 MPa). The detailed procedure of the sample preparation is illustrated in Figure 2 (the laboratory temperature is kept constant during the process of the sample preparation). Although we have tried our best to minimize the impact on the sample during the sampling process, the possible impact of unloading (the sample is reduced from in situ stress to atmospheric pressure after coring) cannot be avoided.

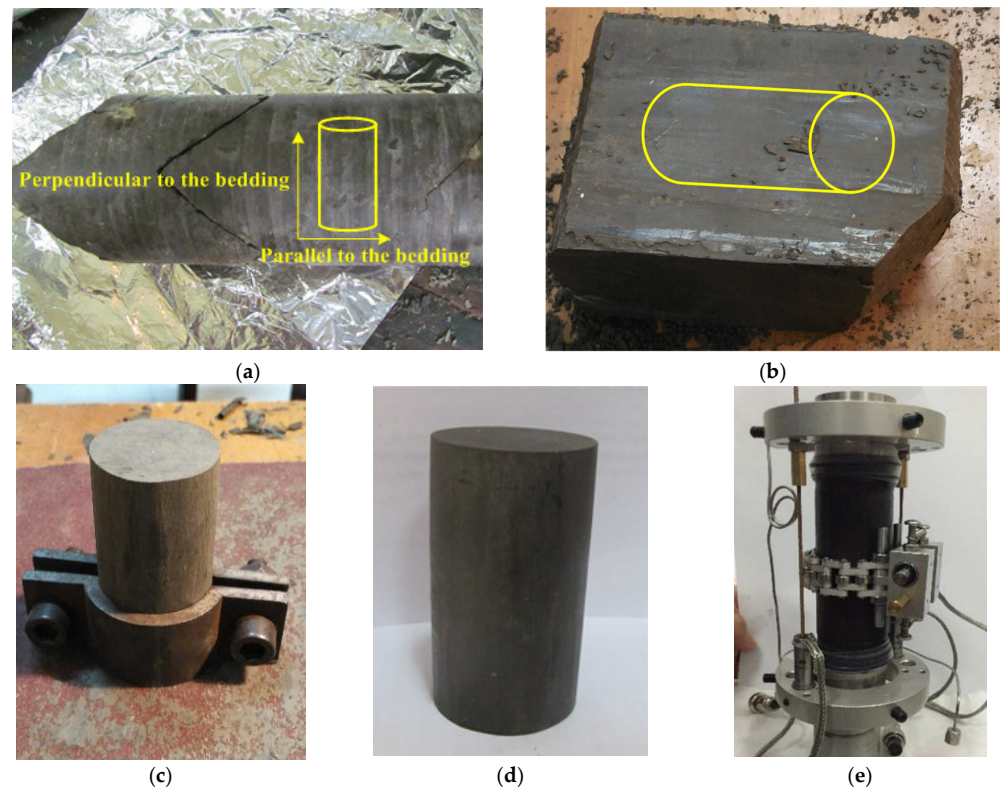


Figure 2. The detailed procedure of hand-trimming: (a) claystone core; (b) pre-cut prism; (c) grinding the sample; (d) the sample; (e) sealing the sample.

The initial physical characteristics of the samples were measured and displayed, as shown in Table 2.

Table 2. Initial condition for the tested samples.

| Number | Height (mm) | Diameter (mm) | Density (g/cm ³) | Dry Density (g/cm ³) | Water Content | Void Ratio | Initial Saturation |
|------------|-------------|---------------|------------------------------|----------------------------------|---------------|------------|--------------------|
| Sample one | 76.26 | 38.36 | 2.02 | 1.68 | 20.68% | 0.64 | 89.06% |
| Sample two | 75.81 | 37.81 | 2.03 | 1.69 | 19.46% | 0.63 | 80.28% |

The claystone samples in this paper were relatively homogeneous (Figure 2b). Yu et al. [1] revealed the micro-structure and composition of the same claystone through scanning electron microscopic (SEM) tests and X-ray diffraction tests. In detail, the particles, most of which are clay mineral crystal particles with pores and are in contact from edge to face or face to face, are bending flaky structures [1]. The main composition of them are shown in Table 3 [1].

Table 3. The main composition of the claystone [1].

| Mineral Composition | Illite | Kaolinite | Illite-Smectite Mix Layer | Chlorite | Quartz | Calcite, Dolomite | Feldspar |
|---------------------|--------|-----------|---------------------------|----------|--------|-------------------|----------|
| Proportion (%) | 15 | 15 | 20 | 25 | 15 | 6 | 4 |

2.3. Test Procedures

The experimental procedures are as follows:

1. A confining pressure of 0.1 MPa was applied to establish the initial system stabilization (about 24 h).
2. The confining pressure was increased to 2.5 MPa at a low rate of 1.68 kPa/min. The volume changes were monitored by a measuring system.
3. The water was thus injected into the samples from the top and bottom. Then, the pore pressure and confining pressure were simultaneously increased by 0.2 MPa at the rate of 1.68 kPa/min.
4. Simultaneous increases of both the confining pressure to 3.5 MPa and pore pressure to 1.0 MPa were applied. The loading rate was controlled at 0.2 kPa/min.
5. Then Skempton's coefficient B was checked to determine the saturation degree of the samples by the following method:
 - Closing the drainage valve.
 - Increasing confining pressure of 0.2 MPa.
 - Measuring the increase in the corresponding pore pressure.
 - Decreasing the confining pressure down to 3.5 MPa and calculating Skempton's coefficient B.
 - Checking Skempton's coefficient B repeatedly until it was greater than 0.85.
6. Keeping the drainage valve open, the effective stress coefficient of claystone was tested in line with the following steps:
 - Increasing the confining pressure by n MPa ($n = 0, 0.1, 0.14, 0.16, 0.18, 0.2, 0.22$), and the pore pressure by 0.2 MPa simultaneously. Then the confining pressure and pore pressure were restored to the previous state ($\sigma_c = 3.5$ MPa, $\sigma_p = 1.0$ MPa).
 - Observing and recording the deformation of samples.

In addition to the above test of the effective stress coefficient, this study also attempted to explore the influence of other potential factors (the neutral stresses and loading rate) on the effective stress coefficient. Different loading rates (0.01 kPa/s, 0.02 kPa/s, and 0.04 kPa/s) and a new pressure increment ($\Delta\sigma_c = \Delta\sigma_p = 0.5$ MPa) were tried in the additional tests.

The variations of confining pressure and pore pressure are illustrated in Figure 3, and the controlled laboratory temperature is shown in Figure 4.

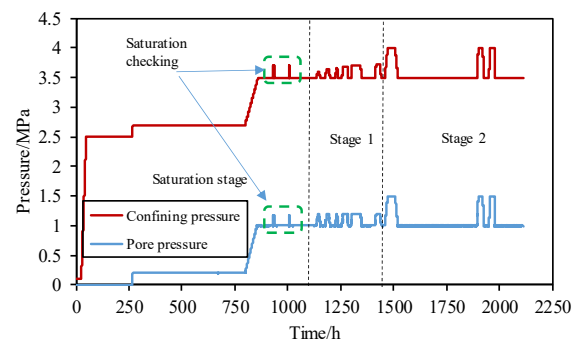


Figure 3. A detailed diagram of the test procedure.

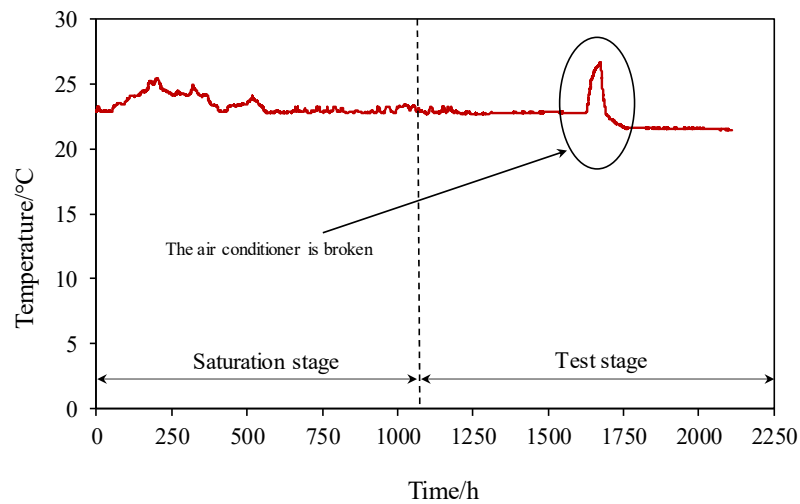


Figure 4. The temperature of the pressure chamber.

3. Results

As shown in Figure 4, the experiments were divided into two stages: the saturation stage at the beginning and the stage of effective stress coefficient determination (the test stage). The following sections will detail the experimental results of each stage.

3.1. Results of the Saturation Stage

After the water was injected into the samples for about one month, Skempton’s coefficient B was checked to determine the saturation degree. The results are shown in Table 4 and Figure 5.

Table 4. The Skempton’s coefficient B for the samples.

| Sample Number | First Time | Second Time |
|---------------|------------|-------------|
| Sample one | 0.913 | 0.925 |
| Sample two | 0.907 | 0.914 |

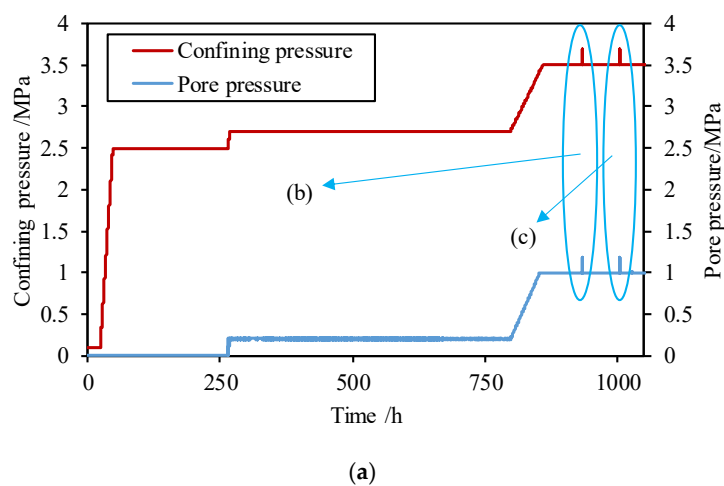


Figure 5. Cont.

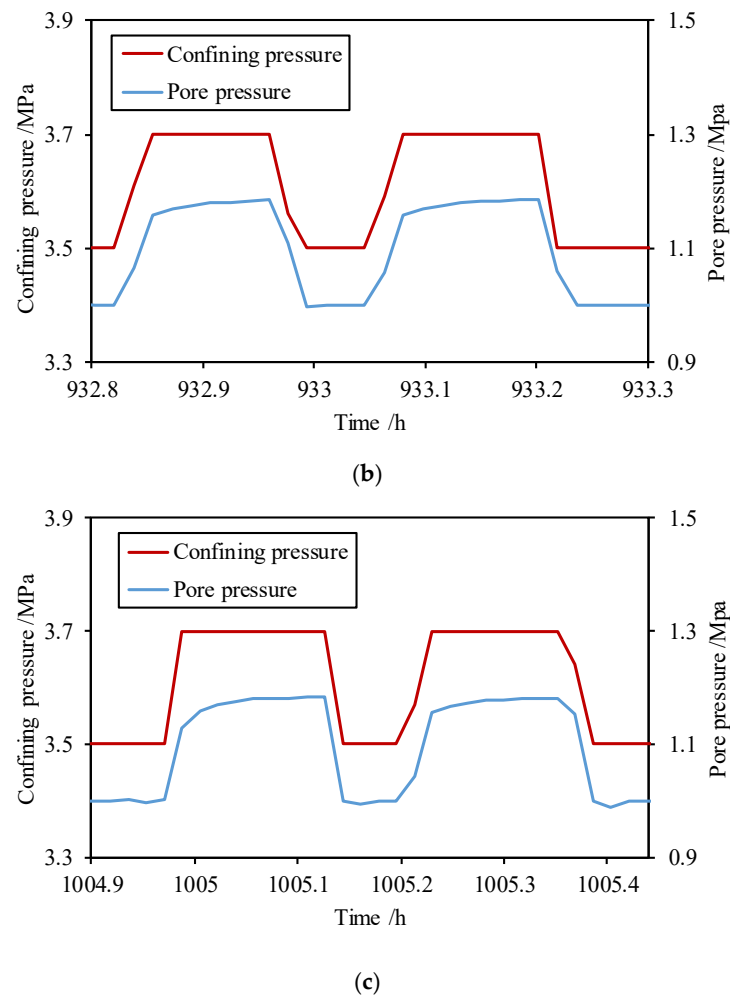


Figure 5. The pressure curve during the saturation testing: (a) the pressure curve during the saturation; (b) testing the saturation for the first time; (c) testing the saturation for the second time.

Usually, Skempton's coefficient B is below one [25,26]. Therefore, it was assumed that claystone was saturated as long as Skempton's coefficient B greater than 0.85. Therefore, sample one and sample two were considered to be saturated. It is worth mentioning the following: (1) the claystone studied in this paper can reach saturation in about 20 days [27]; (2) the saturation of the samples were determined after all the tests, and the results showed that the samples were saturated.

3.2. Results of the Test Stage

The test stage was also divided into two stages (Figure 3): the aim of Stage one was to determine the effective stress coefficient, and the aim of Stage two was to study the effect of the potential influencing factors (the neutral stress and loading rate) on the effective stress coefficient.

3.2.1. Results of Stage One

During Stage one, the pore pressure was always increased by 0.2 MPa at a rate of 0.01 kPa/s. However, different increments were tried for the confining pressure. Meanwhile, different increasing rates were used for the confining pressure to make the confining pressure and pore pressure reach their peak values simultaneously. The variations of the pressures and strains during Stage one are recorded in Figure 6 (negative values represent expansion, whereas positive values represent compression).

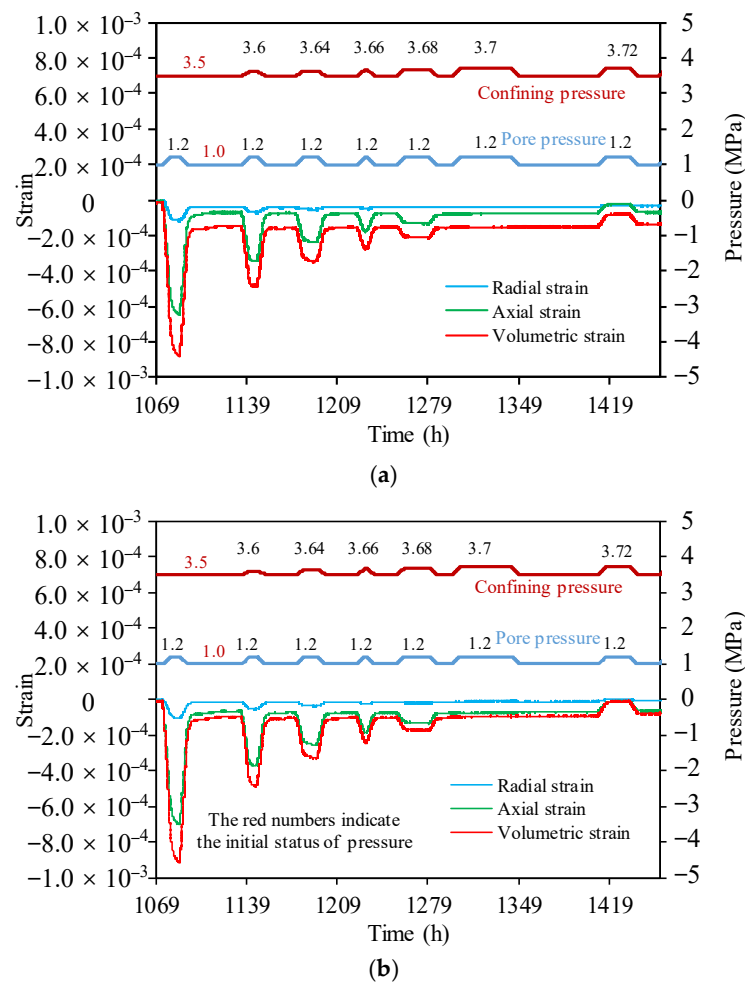


Figure 6. The pressures and strains curve during Stage one: (a) sample one; (b) sample two.

It is well known that effective stress acts on the skeleton directly. When the effective stress changes, the skeleton will undergo corresponding deformation, which is manifested as when the effective stress decreases, the skeleton of the claystone will expand outwards, and the internal pores will be filled with more water; when the effective stress increases, the framework of the claystone will be compressed, and the pore water will be squeezed out.

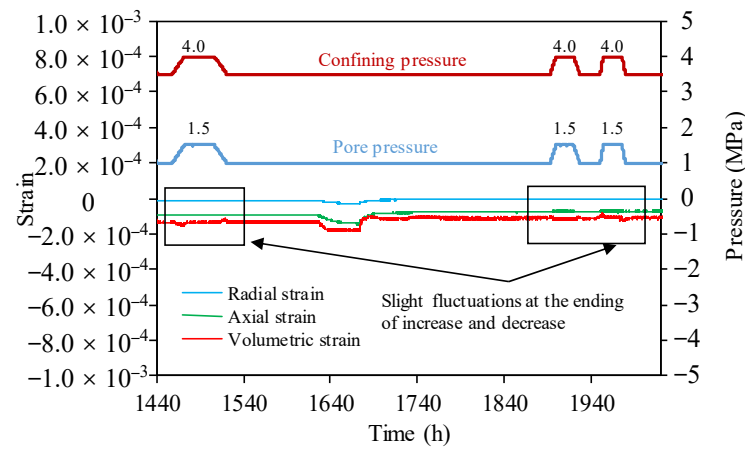
An obvious law summarized by the test data is illustrated in Figure 6:

- (1) The samples undergo a significant expansion when the increment of pore pressure $\Delta\sigma_p = 0.2, 0.2, 0.2, 0.2, 0.2$ MPa is greater than the increment of confining pressure $\Delta\sigma_c = 0, 0.1, 0.14, 0.16, 0.18$ MPa; This means that the effective stress is reduced under this confining and pore pressure condition.
- (2) Conversely, when $\Delta\sigma_p = 0.2$ MPa is less than $\Delta\sigma_c = 0.22$ MPa, these samples are compressed; This means that the effective stress is increased under this confining and pore pressure condition.
- (3) The deformation of the samples are hardly observed when $\Delta\sigma_p = 0.2$ MPa and $\Delta\sigma_c = 0.2$ MPa are equal; This means that the effective stress is constant under this confining and pore pressure condition.

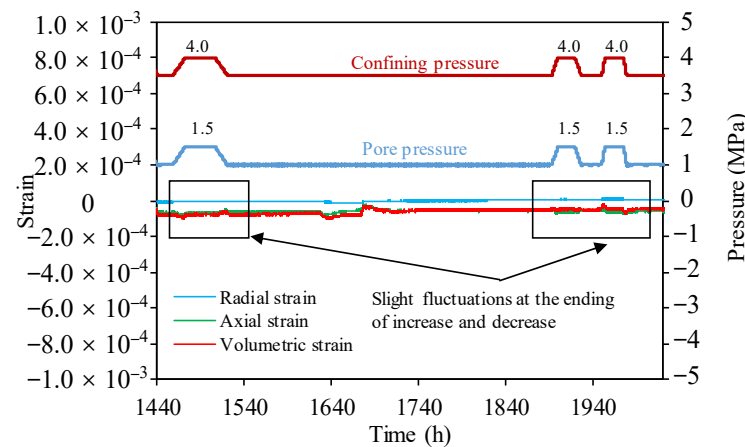
3.2.2. Results of Stage Two

At this stage, the increments of pore pressure and confining pressure were 0.5 MPa, and the loading/unloading rate was 0.01 kPa/s during the first cycle; the increments of pore pressure and confining pressure during the second and last cycles were the same as the first,

but the loading/unloading rates were 0.02 kPa/s and 0.04 kPa/s, respectively. The variations in the pressures and strains during the whole of Stage two are recorded in Figure 7.



(a)



(b)

Figure 7. The pressures and strains curve during Stage two: (a) sample one; (b) sample two.

The results showed the following:

- (1) There were slight fluctuations at the end of the loading and unloading. The reason for this phenomenon is that it was impossible to increase or decrease the pore pressure and confining pressure completely simultaneously.
- (2) The sudden jitter of the strain under stable stress conditions between the first and second cycles was due to a temperature fluctuation (Figure 4).
- (3) The deformations of the samples were all not obvious when the pore pressure and confining pressure were both increased or decreased by 0.5 MPa at a rate of 0.01 kPa/s, 0.02 kPa/s, and 0.04 kPa/s, because pore water could dissipate in time and no excess pore pressure would occur.

4. Discussion on the Effective Stress Principle for Saturated Claystone

4.1. The Value of Effective Stress Coefficient for Claystone

The incremental form of Equation (2) can be written as follow:

$$\Delta\sigma_e = \Delta\sigma_c - \eta\Delta\sigma_p \quad (3)$$

where $\Delta\sigma_e$ is the increment of effective stress; $\Delta\sigma_c$ is the increment of confining pressure; $\Delta\sigma_p$ is the increment of pore pressure.

The largest linear elastic deformation of the samples during Stage one can be obtained from Figure 6 (Table 5).

Table 5. The largest linear elastic deformation of the two samples during each cycle.

| The Number of Cycles | Deformation of Sample One | | | Deformation of Sample Two | | |
|----------------------|---------------------------|---------------|-------------------|---------------------------|---------------|-------------------|
| | Axial Strain | Radial Strain | Volumetric Strain | Axial Strain | Radial Strain | Volumetric Strain |
| The first | −4.95 | −0.81 | −6.57 | −5.24 | −0.73 | −6.70 |
| The second | −2.36 | −0.23 | −2.82 | −2.46 | −0.30 | −3.06 |
| The third | −1.36 | −0.07 | −1.50 | −1.49 | −0.17 | −1.83 |
| The fourth | −0.89 | −0.07 | −1.03 | −1.01 | −0.10 | −1.21 |
| The fifth | −0.45 | −0.02 | −0.49 | −0.51 | −0.03 | −0.57 |
| The sixth | ≈0 | ≈0 | ≈0 | ≈0 | ≈0 | ≈0 |
| The last | 0.46 | 0.08 | 0.62 | 0.47 | 0.11 | 0.69 |

Note: Negative values represent expansion; positive values represent compression; the unit of these strains are 10^{−4}.

- (1) When $\Delta\sigma_p = 0.2$ MPa and $\Delta\sigma_c = 0.18$ MPa, the samples are dilatant, meaning $\Delta\sigma_e < 0$ under this stress condition.
- (2) When $\Delta\sigma_p = 0.2$ MPa and $\Delta\sigma_c = 0.22$ MPa, the samples are compressed, meaning $\Delta\sigma_e > 0$ under this stress condition.

Substituting the above results into Equation (3) gives the following:

$$\left. \begin{aligned} 0.18 - 0.2\eta < 0 \\ 0.22 - 0.2\eta > 0 \end{aligned} \right\} \Rightarrow 0.9 < \eta < 1.1 \tag{4}$$

Berryman [11] presented that the effective stress coefficient of homogeneous rock was not expected to exceed one. Thus, Equation (4) evolves into $0.9 < \eta < 1.0$.

- (3) When $\Delta\sigma_p = 0.2$ MPa and $\Delta\sigma_c = 0.2$ MPa, the deformation of samples are not obvious, meaning $\Delta\sigma_e \approx 0$ under this condition.

Then the following equation is deduced:

$$0.2 - 0.2\eta \approx 0 \Rightarrow \eta \approx 1 \tag{5}$$

The above conclusions indicate that η is a value greater than 0.9 and less than but close to 1.

The effective stress coefficient will be further analyzed according to the above conclusions. The relationship between the stress increments and axial strain increments can be expressed by a generalized Hooke’s law:

$$\Delta\varepsilon_z = \frac{1}{E_v} [\Delta\sigma_z^e - \nu_{vh}(\Delta\sigma_x^e + \Delta\sigma_y^e)] \tag{6}$$

where $\Delta\varepsilon_z$ in the axial strain increment; $\Delta\sigma_x$, $\Delta\sigma_y$, and $\Delta\sigma_z$ are the effective stress increments in x, y, and z direction; E_v is the vertical elastic modulus; ν_{vh} is the Poisson ratio in the horizontal and vertical plane.

According to the results of the stress (Figure 6) and strain (Table 5) variations, the back analysis was performed to determine the effective stress coefficient. The FMINSEARCH function of MATLAB (version number: 8.3) was selected for the optimization calculation. The optimization calculation process is shown in Figure 8, and the objective function of the back analysis can be expressed as the following:

$$\sum_{i=1}^n \left\{ \Delta\varepsilon_{zi} - \frac{1}{E_v} [\Delta\sigma_{zi}^e - \nu_{vh}(\Delta\sigma_{xi}^e + \Delta\sigma_{yi}^e)] \right\}^2 \rightarrow \min \tag{7}$$

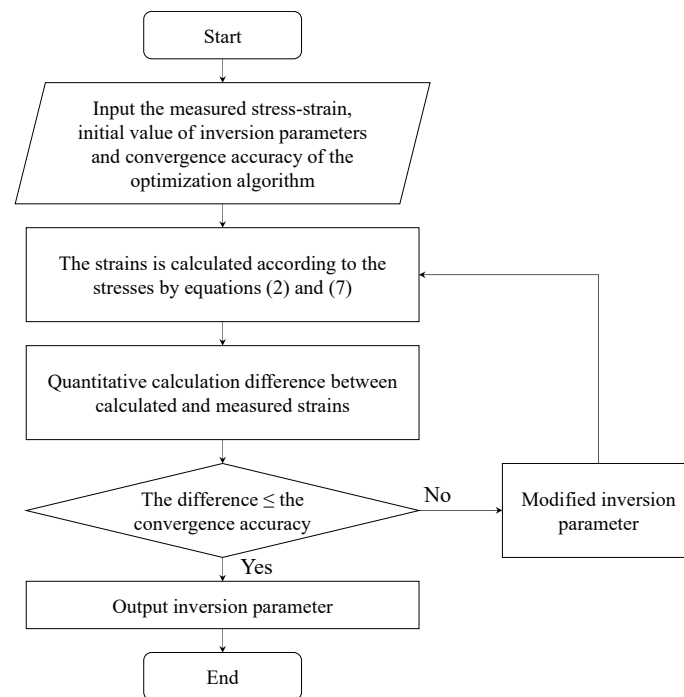


Figure 8. Optimization calculation flow diagram.

To ensure the accuracy of this back analysis, the range of physical parameters is shown in Table 6.

Table 6. The range of physical parameters before back analysis [28].

| Physical Parameters | E_v /MPa | V_{vh} | η |
|---------------------|------------|----------|---------|
| Range | 300–800 | 0.1–0.3 | 0.9–1.0 |

The analysis results showed that the effective stress coefficient of claystone was 0.991 for sample one and 0.995 for sample two.

4.2. Discussion on the Influencing Factors of Effective Stress Coefficient

The effective stress coefficient of claystone was probably related to the testing conditions.

The results of Section 3.2.2 showed that the deformations of the samples were not obvious when $\Delta\sigma_c = \Delta\sigma_p = 0.5$ MPa under different loading rates (0.01 kPa/s, 0.02 kPa/s, 0.04 kPa/s), indicating that the effective stress coefficient of claystone was still close to 1 even if different pressure increments and loading rates were taken. Therefore, the following conclusion can be drawn:

- (1) Whether the testing condition was $\Delta\sigma_c = \Delta\sigma_p = 0.2$ MPa or $\Delta\sigma_c = \Delta\sigma_p = 0.5$ MPa, the results were the same. It means that the neutral stresses may have little effect on the determination of the effective stress coefficient for claystone.
- (2) The results with different loading rates showed an inconspicuous deformation. We may conclude that as long as the loading rates are low enough so that the pore pressure can be dissipated time-efficiently, it will not affect the effective stress coefficient of claystone.

5. Conclusions

The effective stress principle of claystone was studied using the CD tests in this paper.

1. Several loading–unloading cycles were conducted on the saturated claystone samples, and the deformation during this procedure was recorded. The results showed that

both of the two samples were dilatant when the increments of pore pressure were greater than the increments of confining pressure; conversely, these samples were compressed when the increments of pore pressure were less than the increments of confining pressure; finally, the deformation of the sample was hardly observed when the increments of pore pressure and confining pressure were equal. The conclusion is that the effective stress coefficient of claystone is close to one.

2. The relationship between effective stress and strain was analyzed to determine the effective stress coefficient of claystone. The results showed that the coefficient was 0.991 for sample one and 0.995 for sample two.
3. The relationship between the effective stress coefficient of claystone and the potential influencing factors (the neutral stress and loading rate) were studied. The results show that the neutral stress and loading rate may have little effect on the effective stress coefficient of claystone.

Author Contributions: Conceptualization, F.L. and W.C.; methodology, F.L.; validation, F.L., W.C. and Z.W.; formal analysis, F.L.; investigation, F.L.; resources, H.Y.; data curation, M.L.; writing—original draft preparation, F.L.; writing—review and editing, W.C. and Z.Z.; visualization, F.L.; supervision, F.Z.; project administration, W.C.; funding acquisition, W.C. All authors have read and agreed to the published version of the manuscript.

Funding: This research was funded by The National Natural Science Foundation of China, grant numbers 51879258 and 42377179.

Institutional Review Board Statement: Not applicable.

Informed Consent Statement: Not applicable.

Data Availability Statement: Data are available upon request.

Conflicts of Interest: Authors Fanfan Li, Zhigang Wu, Ming Li and Zhifeng Zhang were employed by the company ATCDI (Anhui Transport Consulting & Design Institute CO., LTD). The remaining authors declare that the research was conducted in the absence of any commercial or financial relationships that could be construed as a potential conflict of interest.

References

1. Yu, H.D.; Chen, W.Z.; Jia, S.P.; Cao, J.J.; Li, X.L. Experimental study on the hydro-mechanical behavior of Boom clay. *Int. J. Rock Mech. Min. Sci.* **2012**, *53*, 159–165. [[CrossRef](#)]
2. Ghabezloo, S.; Sulem, J.; Guédon, S.; Martineau, F. Effective stress law for the permeability of a limestone. *Int. J. Rock Mech. Min. Sci.* **2009**, *46*, 297–306. [[CrossRef](#)]
3. Biot, M.A. General theory of three-dimensional consolidation. *J. Appl. Phys.* **1941**, *12*, 155–164. [[CrossRef](#)]
4. Skempton, A.W. *Selected Papers on Soil Mechanics*; Thomas Telford Publishing: London, UK, 1984.
5. Taghizadeh, R.; Goshtasbi, K.; Manshad, A.K.; Ahangari, K. Geomechanical and thermal reservoir simulation during steam flooding. *Struct. Eng. Mech.* **2018**, *66*, 505–513. [[CrossRef](#)]
6. Sonmezer, Y.B. Energy-based evaluation of liquefaction potential of uniform sands. *Geomech. Eng.* **2019**, *17*, 145–156. [[CrossRef](#)]
7. Lee, H.; Oh, T.M.; Park, C. Analysis of permeability in rock fracture with effective stress at deep depth. *Geomech. Eng.* **2020**, *22*, 375–384. [[CrossRef](#)]
8. Guerriero, V.; Mazzoli, S. Theory of effective stress in soil and rock and implications for fracturing processes: A review. *Geosciences* **2021**, *11*, 119. [[CrossRef](#)]
9. Nur, A.; Byerlee, J.D. An exact effective stress law for elastic deformation of rock with fluids. *J. Geophys. Res.* **1971**, *76*, 6414–6419. [[CrossRef](#)]
10. Zoback, M.D.; Byerlee, J.D. Permeability and effective stress. *AAPG Bull.* **1975**, *59*, 154–158. [[CrossRef](#)]
11. Berryman, J.G. Effective stress for transport properties of inhomogeneous porous rock. *J. Geophys. Res. Solid Earth* **1992**, *97*, 17409–17424. [[CrossRef](#)]
12. Tuncay, K.; Corapcioglu, M.Y. Effective stress principle for saturated fractured porous media. *Water Resour. Res.* **1995**, *31*, 3103–3106. [[CrossRef](#)]
13. George, J.D.; Barakat, M.A. The change in effective stress associated with shrinkage from gas desorption in coal. *Int. J. Coal Geol.* **2001**, *45*, 105–113. [[CrossRef](#)]
14. Kwon, O.; Kronenberg, A.K.; Gangi, A.F.; Johnson, B. Permeability of Wilcox shale and its effective pressure law. *J. Geophys. Res. Solid Earth* **2001**, *106*, 19339–19353. [[CrossRef](#)]

15. Tsuji, T.; Tokuyama, H.; Pisani, P.C.; Moore, G. Effective stress and pore pressure in the Nankai accretionary prism off the Muroto Peninsula, southwestern Japan. *J. Geophys. Res. Solid Earth* **2008**, *113*, 401. [[CrossRef](#)]
16. Bagherieh, A.R.; Khalili, N.; Habibagahi, G.; Ghahramani, A. Drying response and effective stress in a double porosity aggregated soil. *Eng. Geol.* **2009**, *105*, 44–50. [[CrossRef](#)]
17. Nowamooz, H.; Ho, X.N.; Chazallon, C.; Hornych, P. The effective stress concept in the cyclic mechanical behavior of a natural compacted sand. *Eng. Geol.* **2013**, *152*, 67–76. [[CrossRef](#)]
18. Konrad, J.M.; Lebeau, M. Capillary-based effective stress formulation for predicting shear strength of unsaturated soils. *Can. Geotech. J.* **2015**, *52*, 2067–2076. [[CrossRef](#)]
19. Zhang, C.L. Examination of effective stress in clay rock. *J. Rock Mech. Geotech. Eng.* **2016**, *9*, 479–489. [[CrossRef](#)]
20. Saurabh, S.; Harpalani, S. The effective stress law for stress-sensitive transversely isotropic rocks. *Int. J. Rock Mech. Min. Sci.* **2018**, *101*, 69–77. [[CrossRef](#)]
21. Ma, J.; Querci, L.; Hattendorf, B.; Saar, M.; Kong, X.Z. The effect of mineral dissolution on the effective stress law for permeability in a tight sandstone. *Geophys. Res. Lett.* **2020**, *47*, e2020GL088346. [[CrossRef](#)]
22. Civan, F. Effective-stress coefficients of porous rocks involving shocks and loading/unloading hysteresis. *SPE J.* **2021**, *26*, 44–67. [[CrossRef](#)]
23. Zhao, Z.; Chen, S.; Chen, Y.; Yang, Q. On the effective stress coefficient of single rough rock fractures. *Int. J. Rock Mech. Min. Sci.* **2021**, *137*, 104556. [[CrossRef](#)]
24. Dehandschutter, B.; Vandycke, S.; Sintubin, M.; Vandenberghe, N.; Wouters, L. Brittle fractures and ductile shear bands in argillaceous sediments: Inferences from Oligocene Boom Clay (Belgium). *J. Struct. Geol.* **2005**, *27*, 1095–1112. [[CrossRef](#)]
25. Mesri, G.; Adachi, G.; Ullrich, C.R. Pore-pressure response in rock to undrained change in all-round stress. *Géotechnique* **1976**, *26*, 317–330. [[CrossRef](#)]
26. Dropek, R.K.; Johnson, J.N.; Walsh, J.B. The influence of pore pressure on the mechanical properties of Kayenta sandstone. *J. Geophys. Res. Solid Earth* **1978**, *83*, 2817–2824. [[CrossRef](#)]
27. Yu, H.D.; Chen, W.Z.; Gong, Z.; Ma, Y.S.; Chen, G.J.; Li, X.L. Influence of temperature on the hydro-mechanical behavior of Boom Clay. *Int. J. Rock Mech. Min. Sci.* **2018**, *108*, 189–197. [[CrossRef](#)]
28. Chen, G.J.; Sillen, X.; Verstricht, J.; Li, X.L. ATLAS III in situ heating test in boom clay: Field data, observation and interpretation. *Comput. Geotech.* **2011**, *38*, 683–696. [[CrossRef](#)]

Disclaimer/Publisher’s Note: The statements, opinions and data contained in all publications are solely those of the individual author(s) and contributor(s) and not of MDPI and/or the editor(s). MDPI and/or the editor(s) disclaim responsibility for any injury to people or property resulting from any ideas, methods, instructions or products referred to in the content.